



**HAL**  
open science

## POD analysis of oscillating grid turbulence in water and shear thinning polymer solution

Tom Lacassagne, Serge Simoëns, Mahmoud El Hajem, Jean-yves Champagne

### ► To cite this version:

Tom Lacassagne, Serge Simoëns, Mahmoud El Hajem, Jean-yves Champagne. POD analysis of oscillating grid turbulence in water and shear thinning polymer solution. *AIChE Journal*, 2021, 67 (1), 10.1002/aic.17044 . hal-03131585

**HAL Id: hal-03131585**

**<https://hal.science/hal-03131585v1>**

Submitted on 2 Nov 2021

**HAL** is a multi-disciplinary open access archive for the deposit and dissemination of scientific research documents, whether they are published or not. The documents may come from teaching and research institutions in France or abroad, or from public or private research centers.

L'archive ouverte pluridisciplinaire **HAL**, est destinée au dépôt et à la diffusion de documents scientifiques de niveau recherche, publiés ou non, émanant des établissements d'enseignement et de recherche français ou étrangers, des laboratoires publics ou privés.

3 **POD analysis of oscillating grid turbulence in**  
4 **water and shear thinning polymer solution**

5 **Tom Lacassagne<sup>1,2\*</sup> | Serge Simoëns<sup>1</sup> | Mahmoud EL  
Hajem<sup>1</sup> | Jean-Yves Champagne<sup>1</sup>**

<sup>1</sup>Univ Lyon, INSA de Lyon, Ecole Centrale de Lyon, Université Lyon 1, CNRS, LMFA UMR 5509, 69621 Villeurbanne Cedex, France

<sup>2</sup>Department of Mechanical Engineering, University College London, Torrington Place, London, WC1E 6BT, UK

**Correspondence**

Tom Lacassagne, Univ Lyon, INSA de Lyon, Ecole Centrale de Lyon, Université Lyon 1, CNRS, LMFA UMR 5509, 69621 Villeurbanne Cedex, France  
Email: tom.lacassagne@gmail.com

**Present address**

\*Department of Mechanical Engineering, University College London, Torrington Place, London, WC1E 6BT, UK

**Funding information**

Oscillating grids are frequently used with water and Newtonian fluids to generate controlled turbulence and mixing. Yet, their use with shear thinning fluids still requires experimental characterization. Proper Orthogonal Decomposition (POD) is applied to PIV measurements of the flow generated by an oscillating grid in water and a shear thinning Dilute Polymer Solution (DPS) of Xanthan Gum. The aims are to investigate the ability of POD to isolate periodic flow structures, and to use it to describe the effects of the shear thinning property. A dominance of the low order POD modes is evidenced in DPS. The methods applied in blade stirred tanks to identify oscillatory motion fail here. However, a strong mode coupling in the grid swept region is observed, determined by the working fluid and by an underlying chaotic nature of the flow. Possibilities of reconstructing turbulence properties using high order modes are discussed.

**KEYWORDS**

POD, shear-thinning, PIV, Oscillating Grid Turbulence

6 **1 | INTRODUCTION AND BACKGROUND**

7 Improving the understanding of the flow dynamics of non-Newtonian fluids is a current goal for many industrial and  
8 environmental applications. In particular, turbulence in non-Newtonian liquids occurs in several industrial applications  
9 for the food or pharmaceutical industries <sup>1,2</sup>. For example, bacteria fermentation for the production of vaccines requires

the stirring of liquid media with a rheology transitioning from a low viscosity Newtonian behaviour to a high viscosity, shear thinning and viscoelastic behavior<sup>3,4</sup>. The level of understanding has not reached that of turbulence in Newtonian fluid yet. This is mostly because of flow interactions with suspended matter giving the fluid its non-Newtonian properties are multiple and complex, and strongly depend on the microscopic nature and properties of this suspended matter. Nevertheless, it is of great importance to improve the understanding of turbulence in non-Newtonian media, since it influences other physical phenomena present in such industrial processes such as passive or reactive scalar mixing, cells growth, or multi-phase mass transfers.

The best way to achieve this, is through fundamental approaches, such as laboratory experiments or numerical simulations. In both type of studies, the situation is often simplified, in terms of geometry and mean flow features, compared to real life conditions, so that the focus can be made on turbulence alone, or turbulence interacting with other phenomenon. The three keys to a relevant experimental approach are the use of accurate measurement techniques, good modelling of the real-life fluid's complex rheology, and use of an efficient way to generate controlled turbulence with a less intense as possible mean flow.

Optical techniques such as Particle Image Velocimetry (PIV), are good candidates to fulfil the first condition. They further provide instantaneous and multi-point measurement of the liquid phase velocity, and allow to estimate many relevant turbulence properties (fluctuating velocities, length scales, time scales ...). They can however only be used in optically transparent solutions, which restricts the set of fluids that can be studied. Fluids that are not optically transparent need to be modelled, which appeals to the second condition listed above. Model solutions often consist in additives dissolved in Newtonian solvents.

Polymers are widely studied as flow additives because they are at the origin of the non-Newtonian properties of the fluid in many applications, and also because the wide range of existing polymers allows to use them to build model fluids reproducing the behaviours of other non-Newtonian media<sup>5</sup>. A well known feature of dilute polymer solutions is their elasticity, which comes from the ability of polymer molecules to deform and exchange energy with the base flow<sup>6,7,8,9</sup>, and leads to the well known drag reduction phenomenon, among others<sup>10,11</sup>. But polymer solutions also commonly exhibit shear-thinning behaviours<sup>12,13</sup>: the viscosity of the solution decreases with increasing shear rate. This, for example, is known to have an impact on both oscillatory motions and turbulence in stirred tanks<sup>14,4</sup>.

The last condition is most probably the hardest to meet: generating controlled turbulence, if possible with a negligible mean flow, has been the challenge of many research teams in the last 50 years, in Newtonian fluids to begin with, but also by extension in non-Newtonian fluids. Several experimental designs have been developed to try to achieve turbulence with moderate mean flow, for example arrays of randomly actuated jets<sup>15</sup>, rotating grids<sup>16</sup>, or "washing machine" experiments<sup>17</sup>. In this paper, we focus on one of the most easy to design and commonly used in water: oscillating grid turbulence (OGT). This method consists in making a rigid grid oscillate in a fluid initially at rest. It is usually said that the jets and wakes behind the grid's holes and bars interact to generate turbulence<sup>18,19,20,21</sup>, which then diffuses away from the grid. In other words, turbulence comes from the periodic shearing of the fluid by the grid.

Oscillating grid apparatus have been commonly used in experimental fluid mechanics since the seminal works of Thompson and Turner<sup>18</sup> and Hopfinger and Toly<sup>19</sup>. Numerous applications can be found in the literature, among which the study of interactions between turbulence and solid impermeable boundaries<sup>22,23</sup>, of turbulence and gas-liquid mass transfer at a free surface<sup>24,25,21,26,27</sup>, in stratified media<sup>18,19,28,29</sup>, or to study the behavior of bubbles, cells, fibers, and flocculation aggregates suspended in a turbulent liquid phase<sup>30,31,32,33,34</sup>. Oscillating grid stirred tanks are thus tools that allow to generate and study controlled turbulence. They can be used as reference cases to help improve the understanding of conventional (bio)chemical reactors.

The most frequent configuration is that of a grid oscillating vertically in a rectangular section tank with a solid flat bottom and a free surface, and for which the properties of turbulence are studied either above or below the grid

swept region, far enough from the liquid/gas or liquid/solid boundary condition. Thompson and Turner<sup>18</sup> studied several types of grids with different mesh sizes  $M$  and different bar shapes and thickness  $d$ . They showed that the best homogeneity and intensity of turbulence was achieved with square section bars and values of a solidity function  $f_s(d, M) = \frac{d}{M} \left(2 - \frac{d}{M}\right)$  lower than 0.4. These principles have been applied in most oscillating grid experiments ever since.

Moreover, it has been shown by Thompson and Turner<sup>18</sup> and Hopfinger and Toly<sup>19</sup> and confirmed by a wide number of studies<sup>35,24,36,37,38,28,39,21,29</sup> that the Root Mean Square (rms) of turbulent velocity fluctuations decays as one over the distance to the grid average position:

$$\langle u'_z \rangle_{rms} \sim Z^{-n} \quad (1)$$

with  $n = 1$ , and

$$\langle u'_x \rangle_{rms} \sim \langle u'_z \rangle_{rms} \quad (2)$$

where  $u'_z$  and  $u'_x$  are respectively the vertical and horizontal turbulent velocity fluctuations, and  $\langle \cdot \rangle_{rms}$  denotes horizontal average (along  $x$ , on a  $-3M < X < 3M$  span) of ensemble rms values. From an historical perspective, the purpose of such setup has mainly been to generate controlled turbulence away from the grid. As a consequence, until recently<sup>23,40</sup>, no study had focused on oscillatory flows generated by the grid motion in and around its swept region, or on how energy is transferred from the oscillatory forcing to turbulence or mean flow.

The influence of non-Newtonian properties on oscillating grid turbulence has first been studied by Liberzon et al.<sup>41</sup>, Wang et al.<sup>42,43</sup>, who addressed questions on turbulence in viscoelastic solutions. Liberzon et al.<sup>41</sup> observed the propagation velocity of the boundary between turbulent and non-turbulent regions in the grid-stirred tank, at the first instants after the onset of the grid's oscillations. They found that the turbulent/non-turbulent interface moved globally faster in dilute polymer solution than in water. Wang et al.<sup>42</sup> and Wang et al.<sup>43</sup> later used a two oscillating grid system to study the viscoelastic effects of surfactants and dilute polymers on coherent structures of OGT. Using proper orthogonal decomposition (POD), they show that the addition of polymer tends to decrease the small scale effects of turbulence, and that this decrease can not only be attributed to the overall viscosity increase, since it is not associated with a decrease of the turbulent kinetic energy (TKE). Hence the non-Newtonian property of the fluid seems to strongly modify the turbulent spectrum. They show promising results for the use of this method to analyse OGT flow properties in complex fluids such as DPS. It is also worth noting that many studies on fixed (passive) grid turbulence in viscoelastic polymer solutions exist in the literature (see e.g. McComb et al.<sup>44</sup>, Vonlanthen and Monkewitz<sup>45</sup>), but as the shear forcing is not periodic and thus intrinsically different from the one considered in the present work, they will not be reviewed here in details for the sake of brevity.

The behaviour of OGT acting in shear thinning solutions remained unexplored until two of our recent articles<sup>46,40</sup>. It has been showed in<sup>46,2019</sup>Lacassagne et al.Lacassagne, Simoëns, EL Hajem, Lyon, and Champagne that polymer addition tends to promote the mean flow's intensity and structure, and that equation 1 and 2 remains valid for polymer solutions in the dilute entanglement regime with a concentration dependent  $n$  exponent. In Lacassagne et al.<sup>40</sup>, the influence of polymer on oscillatory features of the flow around the grid have been described using a phase resolved measurements approach. Despite its suitability for the analysis of periodic motion, this phase averaged method required the collection of important quantity of data and an elaborate data processing<sup>47,40</sup>. It was also only focused on the grid neighbourhood only, whereas the non phase resolved measurements in<sup>46,2019</sup>Lacassagne et al.Lacassagne, Simoëns, EL Hajem, Lyon, and Champagne studied the bulk flow without considering the near grid region.

POD has been recently used in stirred tanks to identify periodic flows induced by blade motions and study their interactions with mean flows and turbulence<sup>48,14,49</sup>, without having to resort to the previous phase averaged measurements. It is also now established as a quick and efficient tool for the study of turbulent flows<sup>50,48,51,52</sup>.

In this work, POD is thus applied to PIV measurements of OGT in water, and in a shear thinning Xanthan Gum (XG) solution at a 100 ppm concentration. In that way, we shall connect the results of our two existing studies in terms of both oscillatory flow and turbulence, and investigate several aspects related to OGT in water and dilute polymer solution (DPS) through the following key questions:

- Can POD be used to identify organised motion (local coherent structures or flow periodicity), oscillating velocity fluctuations, and turbulence in an oscillating grid stirred tank?
- If so, how can it help understanding the effects of polymer addition on the flow inside and outside of the grid swept region ?

This article comes as a complement to the specific analysis of turbulence properties in the tank<sup>46</sup>, and to the phase resolved analysis of turbulence in the neighbourhood of the grid<sup>40</sup> both also presented in.<sup>53,2018Lacassagne</sup>

## 2 | MATERIAL AND METHODS

### 2.1 | Oscillating grid device

For this study, the grid is placed horizontally in a prismatic tank of inner dimension 277 mm by 277 mm by 550 mm. The walls and the lid of the tank are made of transparent plexiglass to allow flow visualization from various angles. The grid has been made from a plexiglass plate shaped by water jet cutting. It has square section bars of side  $d = 7$  mm and its mesh size is  $M = 35$  mm so that its solidity is  $\Xi = \frac{d}{M} \left(2 - \frac{d}{M}\right) = 0.36$ . This is below the maximum value of  $\Xi_{max} = 0.4$  recommended by Thompson and Turner<sup>18</sup> for optimal homogeneity of such turbulence. Two of its corners are fixed to piston rods driving its oscillations, and the other two corners are connected to vertical rail rods in order to stiffen the grid during its motion. A periodic translation motion is conferred to the grid by a rotary engine used along with a crankshaft system. Oscillations of the grid are started from a fluid initially at rest, at least 30 min before the beginning of any PIV measurements, to ensure that the flow has reached a stationary state before its velocity is measured. Based on the grid oscillation parameters, a grid Reynolds number  $Re_g$  can be defined<sup>39,54</sup>:

$$Re_g = \frac{\rho f S^2}{\mu} \quad (3)$$

where  $\rho$  is the fluid density (equivalent to that of water given the very small mass of polymer added) and  $\mu$  the reference fluid viscosity. The grid oscillation frequency is  $f = 1$  Hz and the stroke is  $S = 45$  mm ( $S/M = 1.28$ ,  $S/d = 6.42$ ). This gives a  $Re_g = 2010$  for water at 20 °C, and  $Re_g = 61$  to 1840 for the DPS taking respectively  $\mu$  as the zero shear rate or infinite shear rate viscosities. It is stressed that since the viscosity is variable, comparison of Newtonian fluid flow with Non Newtonian fluid flow through the Reynolds number can be difficult. In so we give the  $Re_g$  range accessible by the non Newtonian fluid flow. This at least shows that a large part of the non Newtonian fluid flow events (high shear rate / low viscosity events) are in the same order of magnitude as the Newtonian ones.

The distance between the grid average position and the bottom of the tank is  $H_G = 5.5M$ . The tank is filled with fluid up to  $H_{tot} = H_G + H_S = 460$  mm which corresponds to a total volume of fluid of about 35.5 L and a grid-surface

average distance of  $H_S \simeq 7M$ .

## 2.2 | Properties of polymer solutions

Shear-thinning properties are conferred to the liquid by addition of a minute amount of XG into distilled water. Here a concentration of polymer  $C_{XG} = 100$  ppm is used. This concentration is at the limit between dilute and semi dilute entanglement regime for XG solutions<sup>55</sup>: the non-Newtonian behaviour of the flow is dominated by polymer-flow interactions with moderate electrical interactions between polymer chains. The shear thinning behaviour of such a solution is modelled by a Carreau-Yasuda equation

$$\frac{\mu - \mu_{\infty}}{\mu_0 - \mu_{\infty}} = \left(1 + (t_{CY}\dot{\gamma})^a\right)^{\frac{p-1}{a}} \quad (4)$$

With  $\mu_0 = 32.8$  mPa.s the zero shear rate, and  $\mu_{inf} = 1.1$  mPa.s the infinite shear rate Newtonian plateau.  $t_{CY} = 1.58$  s is a characteristic time scale of the polymer,  $p-1=-0.5$  is the shear thinning power law exponent, and  $a =2$  is a parameter accounting for the transition between power law and Newtonian behaviours. The flow curve (viscosity as a function of shear-rate) is provided in supplementary material. Viscoelasticity is checked to be negligible for such a XG concentration (elastic modulus  $G'$  and storage modulus  $G''$  have been measured by oscillatory rheological measurements, and  $G'$  is much lower than  $G''$  for  $C_{XG} = 100$  ppm), as expected<sup>55</sup>.

## 2.3 | PIV measurements

Measurements are performed in the vertical central plane of the grid, in two regions: the close grid region (CG) centred around the grid swept zone (SZ), and the full tank region (FT) between the top of the grid stroke and the bottom of the tank (see figure1). PIV acquisition and processing parameters for close grid and full tank studies are indicated in table 1.

Spurious vectors are removed from PIV fields by applying a threshold of 1.2 on the peak ratio, and replaced using median filtering. It is checked that the proportion of replaced vector is always less than 10% of the total vector number.

The data from CG measurements has been used in<sup>40</sup>2019Lacassagne et al.Lacassagne, Lyon, Simoëns, Hajem, and Champagne for a triple decomposition analysis, and the data from FT measurements has been used in<sup>46</sup>2019Lacassagne et al.Lacassagne, Simoëns, EL Hajem, Lyon, to study the mean flow and turbulence properties between the grid and the free surface. Note that in the CG region, the grid is visible on particle images. This made it possible in our previous work<sup>40</sup> to know its position within the phase of oscillations, calculate phase dependent velocity statistics, and access the fluctuating components of the velocity field through the Reynolds triple decomposition proposed by<sup>56</sup>1970Hussain and Reynolds Here for CG measurements, in order to improve the quality of PIV measurements around the grid, this later is masked out from images before processing, as described in this previous work.

As mentioned in<sup>40</sup>, the smallest Taylor micro-scales of turbulence are found in the water case, for which the viscosity is always the lowest. From the values of integral length-scales and using an homogeneous isotropic turbulence assumption, the Taylor length scales are evaluated to be of 3.17 mm for water, 3.25 mm for a 100 ppm XG solution using a constant viscosity equal to  $\mu_{\infty}$ , and 18.17 mm when using  $\mu_0$  as the scale viscosity. The spatial resolutions reported in table 1 are similar to the microscales. This doesn't allow to evidence energy variations at large wave numbers characteristic of viscoelastic turbulence, and thus limits the analysis to the inertial effects and large scales.

## 2.4 | POD analysis

POD is a linear procedure that decomposes data, here a set of vector fields, into a modal base. It has been used only once to study oscillating grid turbulence<sup>43</sup> in a different setup than the present study (two grids). No conclusion on oscillatory flows in OGT has been drawn from this previous work.

The method applied here for obtaining velocity field decomposition is the snapshot method developed by<sup>571987Sirovich</sup> and explained in detail in several articles<sup>4,51,49</sup>. Its principle is briefly recalled here.

The velocity field, is decomposed into a sum of temporal amplitudes  $\theta$  (in m/s) and spatial modes  $\phi$  (dimensionless):

$$U(x, t) = \sum_{i=1}^N \theta^i(t) \phi^i(x) \quad (5)$$

Where  $N$  is the number of modes needed to properly reconstruct instantaneous velocity fields, typically of the order of 400 – 1000<sup>4</sup>. Instantaneous velocity fields obtained by PIV then have to be reorganized in the form of a sequence of snapshots. To do so, the  $(2 \times R \times C) \times N$  snapshot matrix  $S_M$  is written as a column-wise assembly of instantaneous velocity components, where  $R$  and  $C$  are the number of rows and columns of the two-components, two dimensions  $R \times C$  vector field.

The POD algorithm then searches for the set of modes that gives the optimal approximation of each instantaneous velocity field in a least square sense, while satisfying the condition that each mode has to be orthogonal to all others. According to,<sup>571987Sirovich</sup> this is equivalent to an eigenvalue problem and can be written as

$$R\phi = \lambda\phi \quad (6)$$

Where  $R = \frac{1}{N} S_M (S_M)^T$  is the two point cross correlation matrix between velocity components, and  $\lambda$  (in  $m^2/s^2$ ) is the eigenvalue associated to mode  $\phi$ .  $\lambda$  quantifies the energy content of its associated mode. It is used to sort out the modes from the most to the least energetic.

Once it is done, instantaneous velocity fields can be estimated by reconstruction up to a given number of modes using equation (5) with an order of summation lower than  $N$ . This allows to suppress the small scale of turbulence contribution (high order modes), measurement noise (higher order modes), or even oscillatory motion contributions (coupled and/or oscillatory modes, see the next paragraph). Combination of mode can be used to isolate a relevant set of velocity scales' contribution, assuming that one can give a physical meaning to this collection of modes.

POD has been widely used since the end of the 2000's as an alternative to phase resolved measurements for the identification of trailing vortices and oscillatory flows in stirred tanks<sup>58,48,4,14,51,49</sup>. Its main advantage is that it requires only a small number of velocity field sampled ( $N$  in equation (5)) and no knowledge of the blade position for each recorded field, while phase resolved measurements require complex timing set-ups and the accumulation of much more instantaneous fields in order to achieve statistical convergence for each blade position. By analogy to this blade stirred tank case, applying POD to the oscillating grid flow should provide information on turbulence and coherent structures in a much quicker and less data-consuming fashion than the phase averaged measurements detailed in,<sup>402019Lacassagne et al.Lacassagne, Lyon, Simoëns, Hajem, and Champagne</sup> and identify modes that correspond to the oscillatory component of the flow<sup>42013Gabelle et al.Gabelle, Morchain, Anne-Archard, Augier, and Liné, 142013Liné et al.Liné, Gabelle, Morchain, Anne-Archard, and Augier</sup>

This is one of the main interest of applying POD here. In this work, mean velocity is removed from instantaneous fields prior to POD decomposition, hence the mean flow correspond to mode number 0 (i.e it is not present in the de-

composition). A description of the mean flow in similar conditions is available in Lacassagne et al.<sup>46</sup> and its interactions with periodic and turbulence fluctuations is addressed in Lacassagne et al.<sup>40</sup>. Comparing mean flow velocities reported in the two previous works with and POD decomposition in the GN region, the kinetic energy associated to this mean flow is estimated to be an order of magnitude smaller than the kinetic energy attached to the first POD mode for water, and of the same order of magnitude for the polymer case (for which a mean flow enhancement occurs).

Once mean flow and oscillatory motions are identified, higher order modes remaining should correspond to either turbulence or to some peculiar combinations of interactions of modes or waves. The highest order ones then correspond to noise.

The code used here is the one implemented in DaVis 8 software<sup>60</sup>. The average velocity field over 1000 fields (which are enough for convergence, as demonstrated in<sup>40</sup> and<sup>46</sup>) is computed and subtracted to instantaneous velocity fields. The POD decomposition is then performed over 1000 modes using the double precision option. Lower order reconstruction of velocity fields can then be built using a limited number of modes (from 1 to 1000). If one wants to isolate and describe the behaviour of a specific set of intermediate modes, a partial reconstruction from this set only can be deduced from linear combination of two other reconstructions. For example the partial reconstruction using modes 2 and 3 only is computed as the reconstruction up to mode 3 minus the reconstruction based on mode 1 alone. This combination is made possible by the fact that POD is a linear procedure.

POD is applied, as described above, to three regions of interest (ROI) of the flow in the plane of measurement:

- the swept zone (SZ) which is defined as the area covered by the grid motion, and is available in CG measurements
- the grid neighborhood (GN) defined as the upper part of the CG region minus the swept zone (GN=CG-SZ)
- the full tank (FT) ROI defined in figure 1

Reference phase resolved measurements are available for the CG (GN and SZ) regions in.<sup>40,2019Lacassagne et al.Lacassagne, Lyon, Simoëns, Haj</sup>

## 3 | RESULTS AND DISCUSSION

### 3.1 | POD Modes

The two first  $\phi$  spatial modes (1 and 2) and a higher number mode (chosen arbitrarily as 60) are represented in figure 2 for SZ, GN and FT regions, for water and dilute polymer solution. In both liquids, modes 1 and 2 in the SZ region are structures according to the grid design: 6 regions of high magnitude corresponding to the 6 mesh "holes" are visible. Even though the mean velocity field has been subtracted from instantaneous fields prior to POD decomposition, modes 1 and 2 in the FT region show a magnitude field somehow similar to the mean flow intensity displayed in<sup>46,2019Lacassagne et al.Lacassagne, Simoëns, EL Hajem, Lyon, and Champagne</sup> in both water and DPS. Mode 60 is supposed to be associated with turbulence, since it is a high order mode. Indeed, the structures observed are much smaller than for modes 1 and 2, and their magnitude decays when moving away from the grid. Moreover, in all the three regions, the typical size of a high magnitude patch seems smaller in water than in DPS (see for example mode 60, region SZ in water and DPS). Note since the intensity is carried by the temporal mode coefficients, the above color maps should not be used to compare amplitudes from one mode to another, but only between spatial structures of the modes and spatial distribution of  $\phi$ , as done here.

The above description seems consistent with the general observation that polymer tends to promote larger organized structures and damp the small scales of turbulence and grid turbulence<sup>43</sup>. Turbulence in dilute polymer solutions sees its energy distribution between scales modified. This should be evidenced in the POD decomposition not



only by a modification of the high mode structures, but also by an adaptation of the mode by mode energy distribution.

### 3.2 | Energy distribution

Figure 3 shows the eigenvalue spectrum of POD modes, that is to say the magnitude  $E_{\lambda_i}$  of each modes divided by the sum of all eigenvalues  $\sum_i E_{\lambda_i}$ . This ratio quantifies the portion of total kinetic energy included in each mode. It should however be kept in mind that this concerns the measured kinetic energy, which might not be exactly the total kinetic energy actually present in the flow due to experimental limitations (e.g. planar and two-dimensional measurements).

The first modes are representative of large coherent structures (organized motions) and so contain most of the energy. This is especially the case close to the grid where the grid's motion forces the large structures: the first modes have a higher energy share in the SZ region than in the CG region, and in the CG region than in the FT region. The higher order modes are then said to represent turbulence or noise. According to<sup>612003De Angelis et al.De Angelis, Casciola, Lvov, Piva, and Procaccia, 142013Lin</sup> the eigenvalue value spectrum of a POD decomposition of a turbulent flow presents a  $-11/9$  slope at high modes when plotted on a log-log scale (also plotted on the figure for illustration). The range for which the spectrum follows this slope is here limited. This can be due to two reasons: the relatively low grid Reynolds number which may lead to poor scale separation in all fluids, and the limitations in the spatial resolution of PIV measurements which doesn't allow to describe the smallest turbulent scales (as mentioned previously). However, it seems that this  $-11/9$  slope is reached for lower modes in the FT region, suggesting that such lower modes may there already be related to fine, turbulent scales, as will be confirmed later in the following sections. Note that advanced maximum entropy methods also exist and allow to reconstruct energy density spectra (as a function of wave-number) from POD decomposition and verify their agreement to the conventional  $-5/3$  slope in the inertial turbulence range, as described in Liné<sup>62</sup>.

In the DPS case, this energetic dominance of the first modes seems to be enhanced: the first eigenvalues share is always higher in the non-Newtonian case than in water, and the eigenvalue spectrum curves for DPS and water cross at a given mode. Lower order modes than this crossover values see their energetic share amplified in DPS whereas higher order modes have their impact decreased. This trend can also be visualized by plotting the cumulative energy as a function of the number of modes, as in figure 4. It shows that cumulative energy converges towards its total value quicker in DPS than in water, and that for every region of the flow. Fewer modes are necessary to capture most of the kinetic energy in DPS than in water for a given region of the flow. Energy concentrates in the first few modes. This has also been evidenced by<sup>612003De Angelis et al.De Angelis, Casciola, Lvov, Piva, and Procaccia</sup> while studying the drag reduction of polymers in turbulent channel flows, and by<sup>432016Wang et al.Wang, Cai, Wei, Zhang, Wang, and Li</sup> in two oscillating grid turbulence of viscoelastic fluids.

A final interesting conclusion can be drawn using eigenvalues. By plotting for FT and SZ regions the eigenvalue spectrum of DPS  $E_{\lambda_i}^{DPS}$  normalized by the corresponding eigenvalue spectrum for water  $E_{\lambda_i}^w$  (figure 3 c)), one shows that for the first modes, the energetic enhancement is more significant for the FT region, which does not include the swept zone of the grid. Indeed, the negative slope of  $E_{\lambda_i}^{DPS}/E_{\lambda_i}^w$  is decreased for FT as compared to the slopes of SZ. In other words, the steeper decreasing slope with increasing mode number suggests an even stronger low mode (large scales) enhancement in the FT case regardless of the overall value of the dissipation. This observation leads to the conclusion that the enhancement of energy share of the first mode can not only be attributed to organized motions generated by the grid (which are dominant in SZ region), but is also a feature of turbulence in DPS. It can be that small scales of turbulence are damped by the polymer, as previously observed in previous viscoelastic turbulence studies<sup>6,8</sup> and also using POD analysis<sup>61,43</sup>. This translates into a decrease of the high POD modes energy, that are indicators of these small scales. For regions where the grid forcing is not directly felt (FT), the eigenvalue spectrum is intrinsically flatter (see figure 3) since mean and organized motion caused by the grid are weaker.

In other words, even in Newtonian flows, the energy share is quite balanced between modes in the FT region whereas in the SZ region, energy is more contained in low order modes because of the grid. A damping of small structures is thus more visible in the FT region for which these structures are significant in the flow's energy, than in the SZ region where they are less influential.

All of the above thus to confirm that the shear-thinning behaviour and the proximity to the grid promote large scale flow structures (organized or turbulent).

However, one should keep in mind that the DPS viscosity being always higher than that of water, total kinetic energy dissipation is likely higher. In a Newtonian fluid with viscosity analog to that of DPS, and equivalent total dissipation, smaller scales would be larger than in water. This implies that in such a fluid, a given mode number is already associated to larger flow structures (smaller wave numbers) with intrinsically higher kinetic energy content, owing only to differences in viscosity. When normalising spectra "by mode number", as done in figure 3 c), the effect would thus also be to promote low order modes. It is very difficult to estimate true local dissipation values in shear-thinning fluids, which makes re-scaling of the spectra and normalisation "by wave number" challenging. It is thus possible that the slope observed in figure 3 c) derives from both differences in "Newtonian" viscous dissipation, and small scale damping due to the polymer. The latter alone would have potentially led to still decreasing but flatter slopes.

### 3.3 | Identification of organized motion

Let us recall the criterion for the identification of oscillatory modes of the flow in stirred tanks<sup>14,49,59</sup>, that we shall use as a starting point for our analysis. Oscillatory components are the results of coupled modes for which:

- two successive eigenvalue values are close to each other in the eigenvalue spectrum (the coupled modes have the same energetic impact).
- the temporal coefficient of each mode  $i$ ,  $\theta_i(t)$ , shows a sinusoidal trend when plotted versus time, and its PDF is shaped like that of a sinusoidal function (while that of a turbulent mode approaches a Gaussian shape (as discussed later in figure 6) .
- the scatter plot of two coupled modes arranges in a circle in the  $\theta_i$ - $\theta_{i+1}$  space.

From the eigenvalue spectrum figure 3, no couple of successive eigenvalue of equivalent magnitude can easily be extracted, and that even in the SZ region where oscillatory motion is known to be dominant. The second identification criterion yields better results. Indeed, the plot of temporal coefficient intensity as a function of the field index (approximately replacing here time since the measurements are not time resolved) allows to identify a clear sinusoidal behaviors for the first mode in the SZ region for both water and DPS. Since velocity fields are recorded at 10 Hz and the grid frequency is 1 Hz, a periodicity of  $P = 10$  in terms of field index is quite logically found for this first, principal, periodic mode. Modes 2 and 3 also seem to have a periodic behavior, but with a higher frequency (lower  $P$ ,  $P=5$ ). In the GN region for water, the sinusoidal behavior of mode 1 disappears and no periodic behavior is observed for the following modes. In the GN region for DPS however, an oscillatory behavior can be observed for mode 1 and 3. Yet, due to the quite low time resolution of measurements, higher flow frequencies can not be captured by the plots of figure 5.

The probability density function (PDF) of the values of  $\theta^i$  coefficients over 1000 instantaneous fields for the same set of modes, represented by the histogram plots of figure 6 completes the information on periodic mode behavior. The PDF of mode 10 always approaches a Gaussian shape, characteristic of random distribution. Coefficients  $\theta^1$  for water and DPS in the SZ region have a flat shaped distribution corresponding to their (poorly sampled since not time resolved) sinusoidal like behavior. The PDF of coefficient  $\theta^2$  and  $\theta^3$  also suggest a non-random time distribution of the mode in the

SZ region, and so a possible periodicity. All PDFs in the GN region for water are bell-shaped, which is expected from figure 5. Finally, PDFs of temporal coefficients for modes 1 and 3 in DPS for the GN region also exhibit a quasi-Gaussian shape even if their "time" series plot looks periodic.

To a first approach, all these observations are consistent with the previous remarks based on phase averaged measurements: oscillatory motion can logically be found in the SZ region, but is strongly damped when moving away from the grid, and as a consequence almost invisible in the GN region (for water at least). Polymer has an organizing effect on the flow which tends to promote this oscillatory motion and keep it significant in the vicinity of the grid. However, the distinction between periodic and non periodic modes is sometimes arduous due to the poor temporal resolution of our measurements, and also to the periodic behavior of modes that can be less pronounced than in stirred tanks. A conclusion is that evolution and PDF of  $\theta$  coefficient alone may not be sufficient to identify clearly periodic modes. A complementary step is thus to check the degree of coupling between modes.

No circular arrangement similar to the one found for oscillatory motion in stirred tank can be observed, for any region, fluid, or pair of successive coefficients  $(\theta^i, \theta^{i+1})$ . This is to some extent not surprising since in the stirred tank case, circular organization of the temporal coefficients is evidenced for a pair of successive modes that exhibit an equivalent magnitude in the eigenvalue spectrum, and no such pair of modes is observed here (figure 3). In the SZ region for both water and DPS however, the scatter plots of  $\theta^1$  versus  $\theta^2$  and  $\theta^2$  versus  $\theta^3$  values are not randomly distributed as one would expect for uncoupled modes, but arrange in a more complex characteristic pattern, which can also be seen in three dimension by plotting the 3D scatter plot of  $\theta^1$  versus  $\theta^2$  versus  $\theta^3$  values (see figure 7). The dispersion around those defined patterns is quite small. The  $(\theta^1, \theta^2)$  pattern has a similar infinity symbol shape for water and DPS, with a variation of the two lobes' sizes and of the crossing point location.  $(\theta^2, \theta^3)$  patterns also include two lobes, but are yet quite different in the two fluids. In the GN region, this settlement disappears.

Infinity shapes, translating into 8-shapes when projected on a 2 modes space, could possibly be related to the frequency of one mode being twice that of the second one (e.g modes 1 and 2 for water, figures 5 and 7). Not all mode pairs fit this scenario. For example modes 2 and 3 in DPS display a two lobes structure (and not an 8 shaped one), while the frequency of mode 3 is twice that of mode 2 in figure 5.

In ref,<sup>51</sup>2017Gabelle et al.Gabelle, Morchain, and Liné similar patterns of mode coupling are observed in stirred tanks, and used them to evidence a triadic interaction involved in energy transfer between modes. The observation of figure 7 and the work previously cited still allows to formulate two hypothesis:

- These shapes are a consequence of the strong oscillatory motion observed in the SZ region but not in the GN region, and this motion can not be described by a simple two-mode coupling, but a triadic interaction is likely involved
- The presence of polymer modifies the features of oscillatory motion in the SZ region. This is expressed in POD decomposition by a variation in the coupling between low order modes

The energy transfer between modes likely corresponds to an energy transfer between different types of periodic structures of the flow. In stirred tanks, several types of trailing vortices have been evidenced<sup>49</sup> and exchange energy<sup>51</sup>. The main one is the trailing vortices behind the blades of the impeller. In the oscillating grid system, we know that the main oscillatory motion is composed of alternating jets and wakes around the grid bars and holes, and that a secondary oscillatory motion exists, such as periodic vortices near the walls. The key difference between the topology of the principal oscillatory structures is that in stirred tanks, the trailing vortices always revolves in the same direction whereas in OGT the direction of the periodic motion changes. For a fluid particle in the region of interest the motion induced by the principal periodic motion will always be null or in a given direction, whereas in the OGT case it can be along different direction of the same axis. Moreover, in the stirred tank case, turbulent structures once generated by the blade evade

350 the swept zone and are left to evolve and dissipate freely in its wake, while in the grid-stirred case, eddies generated by  
351 one grid pass almost immediately re-interact with the grid half a period later, making turbulence and periodic structures  
352 strongly coupled.

353 We infer that the triadic coupling comes from the energy transfer between oscillatory component of the flows,  
354 some of which have changing directions or signs. The specific shape of these structures in OGT is yet to be explained. It  
355 could be in some ways linked to an energy transfer efficiency between modes and consequently between flow structures.  
356 An interesting next step would thus be to develop a criterion based on the shape of these patterns to quantify inter  
357 modal energy transfer and see its evolution with stirring conditions (Reynolds number, Deborah number ...).

358 As a last remark, regarding as if subjacent trajectories in the phase space could be induced by such a low order mode  
359 coupling, we can notice similarities with chaotic motion figures in laminar flows<sup>63</sup>. Indeed, the temporal amplitude  $\theta$   
360 patterns in figure 7 a) and c) strongly remind the shape of chaotic attractors. This point could be worth investigating  
361 in order to explain the patterns' shapes. The following question then arises: may those results indicate an underlying  
362 chaotic behaviour in the grid swept zone, possibly issued from a laminar, low grid Reynolds number  $Re_g$ , chaotic process  
363 ? A positive answer to the previous question could for example lead to the observation of specific mixing trends in the  
364 swept region implied by the subjacent chaotic process, or to further mixing at higher concentration of polymer for which  
365 turbulence like traces disappear. Figure 7 could thus be the evidence of a secondary mixing mechanism, possibly chaotic  
366 or at least characterized by complex oscillations, efficient near the grid and in low Reynolds number turbulence-free  
367 flows.

368 As one can see, organized motion is difficult to identify using the common criterion for stirred tanks. In other words,  
369 POD fails to identify unequivocally local coherent structures, but still provides an information on the global periodicity  
370 of the flow through a set of modes. One of the interest of POD is that it makes it possible to reconstruct velocity  
371 field using a specific set of modes. With the objective of identifying purely turbulent motion free of any oscillatory  
372 component, it is thus easy to remove the oscillatory component from non phase resolved measurements, provided that  
373 the modes responsible for oscillatory motion can be identified.

374 From the above, and as an extension of the existing criterion in blade stirred tanks, we suggest that closed patterns  
375 in temporal modes scatter plots could be used as an indicator to unambiguously identify modes involved in oscillatory  
376 motion description. Further investigation on multi-modes coupling patterns, in 3 or more mode dimensions, and how  
377 these patterns project in two mode dimension space (figure 7) is yet still needed.

### 378 | 3.4 | POD reconstruction of turbulence properties (FT)

379 What can still be done in a first approximation is define a threshold mode number for turbulence properties recon-  
380 struction. Indeed it is now admitted that oscillatory motion is described by coupling of low order modes, especially  
381 in the SZ region. In the GN region, even low order modes are difficult to identify as oscillatory and/or coupled using  
382 their temporal amplitude  $\theta$  (see figures 5,6 and 7). By setting a limit number of modes considered to be part of the  
383 oscillatory motion, one implicitly sets a limit under which modes are considered periodic and non-turbulent, and above  
384 which they are considered as turbulent and non periodic. It is thus possible to use high order modes only for the  
385 reconstruction and estimation of turbulence properties, free of any mean or oscillatory motion, but there is a risk  
386 that large scales of turbulence have been artificially removed by suppressing the low order modes. What is proposed  
387 here is to check the influence of low order mode removal on the statistical properties of reconstructed velocity fields.  
388 Partially-reconstructed fluctuating velocity fields are then calculated by subtracting the reduced order models to the  
389 full reconstruction. By this method one gets velocity fields estimated using modes  $M_R + 1$  to 1000. These are denoted  
390 as  $M_{R-end}$  POD reconstructions. In the two following paragraphs, reconstruction is performed in the FT region. The

391 turbulent velocity rms profiles along depth, and the power spectra of turbulence reconstructed using different sets of  
 392 modes are compared.

### 393 3.4.1 | Profiles of rms velocity

394 The rms velocity profiles along the vertical direction are estimated by horizontal averaging over the FT region of  
 395 the rms velocity fields obtained after POD reconstruction. Vertical profiles of  $\left\langle u'_{z, M_R-end} \right\rangle_{rms}$  for water and DPS in  
 396 the FT region are plotted in figure 8, and follow power law shaped decay as expected from equation 1. Profiles for  
 397  $M_R = 1$  are for the vertical velocity fluctuations corresponding to the horizontal velocity fluctuations profiles already  
 398 reported in.<sup>462019Lacassagne et al.Lacassagne, Simoëns, EL Hajem, Lyon, and Champagne</sup> The main effect of low order mode removal  
 399 on reconstructed fields is visible in this figure. It is a decrease of the rms velocities and thus of the TKE. Removing the  
 400 most energetic modes from reconstruction leads to a decrease in the rms of fluctuating velocity. This is not surprising  
 401 since the first POD modes are the ones carrying most of the fluctuating kinetic energy. The effect is even more significant  
 402 in the DPS case where low order modes are associated to a higher energy content. In order to get beyond simple energy  
 403 removal effects, one may consider the profiles of rms velocity  $\left\langle u'_{z, M_R-end} \right\rangle_{rms}$  corrected by the energy loss due to mode

404 removal (figure 8). Here the chosen scaling is a division by a factor  $\sqrt{1 - e}$  where  $e = \frac{1}{100} \frac{\sum_{p=1}^{M_R} E_{\lambda_p}}{\sum_{i=1}^N E_{\lambda_i}}$  is the portion of kinetic

405 energy carried by the removed modes derived from figure 4. The scaling factor  $\sqrt{1 - e}$  thus corresponds to a reference  
 406 velocity built on the total energy carried by the remaining modes. Scaled rms velocity profiles are plotted in figure 8  
 407 b) and d), and are found to collapse for both water and DPS in a single profile with a well defined power law region  
 408 characteristic of oscillating grid turbulence. Removing the first modes before velocity reconstruction does not affect  
 409 the shape of the rms velocity profiles (the n exponent). It means that the contribution of the first modes to the rms  
 410 has the same dependency on the grid distance than that of the following modes, that is to say the one depicted by the  
 411 normalized profile. It either means that the decay law for oscillating velocity fluctuations is the same than the one for  
 412 turbulent velocity fluctuations, or that the first modes are already significantly representatives of turbulence. Here  
 413 the most likely conclusion is that in the FT central region, oscillatory motion is non-existent, or too weak for it to be  
 414 captured efficiently by POD, so that first modes are already indeed turbulent modes. It is worth noting that for this FT  
 415 region, no phase-resolved measurement is available, so there is no way to check that this oscillatory motion is truly not  
 416 present. However phase averaged measurements in the CG region have shown that periodic fluctuations are strongly  
 417 damped when moving away from the grid, and are very low outside of the SZ region in the central part of the tank<sup>40</sup>.  
 418 It is thus not surprising that no oscillatory behaviour is captured by POD in the FT central region. Applying a similar  
 419 reconstruction procedure to the SZ region would probably lead to normalized rms profiles highly dependent on the  
 420 presence or removal of the first POD modes.

### 421 3.4.2 | Turbulence spectra

422 In the FT region, 1D power spectra can be computed from the Fourier transform of the cross correlation coefficient of  
 423 the velocity field. For that purpose, two-point auto-correlation coefficients  $R_i^j(M, r_j)$  are computed for each velocity  
 424 component  $i$ , in each direction  $j$ , with  $r_j$  the distance between M and a second point, and  $i = x$  or  $y$  and  $j = x$  or  $y$ .  
 425 First evaluated at every location M of the ROI, correlation coefficients are then spatially averaged on M over  $x$  and  $y$ ,  
 426 and 1D power spectra  $P_i^j$  computed by Fourier transform of individual correlation coefficient curves  $R_i^j$ . This yields  
 427 power spectrum for the tangential and longitudinal fluctuating velocity components respectively  $P_i = 0.5(P_x^x + P_y^y)$  and

428  $P_t = 0.5(P_x^y + P_y^x)$ . The cumulative power spectrum  $P$  is defined as the sum of the last two<sup>64</sup>. It is plotted in figure 9  
429 for water and DPS using various reconstructions: one including the full set of modes (black dots), some using the first  
430 few modes only ( $M_0 - M_i$ , empty markers), and the complementary reconstructions using the higher order modes only  
431 ( $M_i - end$ , full markers).

432 From figure 9, it can be checked that the low order modes are associated to the lower wave numbers  $k$  hence to the  
433 larger structures of turbulence. Indeed, the empty marker spectra corresponding to reconstructions using only the  
434 low order modes are dominant at low  $k$  values but quickly decrease with increasing  $k$ . For  $k > 2 \cdot 10^2$  typically, spectra  
435 build on higher order modes (full markers) are superimposed with the one reconstructed on the full set of modes. It  
436 indicates that at these wave numbers, turbulence can be described by the higher order modes only.

437 For low wave numbers, fully reconstructed spectra are better matched by the partial reconstructions using high  
438 order modes. Yet in the previous paragraph, it was shown that these low order modes are not likely oscillatory or  
439 periodic components of the flow. They should thus already correspond to large, random, turbulent structures. This last  
440 assumption can be checked by looking at the slopes of the power spectra at low wave numbers in figure 9. The energy  
441 input by the grid occurs at large spatial scales, described by low wave numbers of magnitude between  $1/S$  and  $1/M$   
442 (dashed/dotted vertical lines) corresponding respectively to one over the amplitude of oscillations and one over the  
443 mesh parameter. With increasing wave numbers, the fully reconstructed power spectrum gradually tends to a  $-5/3$  slope  
444 trend characteristic of the inertial sub-range of turbulence. It is worth noting that the turbulence Reynolds numbers  
445 used here are quite low (Taylor based Reynolds number around 30) and it is not surprising that this  $-5/3$  slope is not well  
446 developed on the measured spectra. Yet an important observation on POD reconstruction can be made: when removing  
447 first order modes from the reconstruction, the wave number range in which the slope of power spectra approaches this  
448  $-5/3$  value is reduced, and pushed away to the high wave number range. For example, the  $M_0 - end$  spectrum in DPS  
449 only roughly fits the theoretical slope in the  $k \in [2 \cdot 10^2, 6 \cdot 10^2] \text{ m}^{-1}$  region while the fully reconstructed spectrum follows  
450 this trend in  $k \in [6 \cdot 10^1, 2 \cdot 10^2] \text{ m}^{-1}$  as well.

451 Removing the first order modes from POD reconstruction in this case thus corresponds to artificially removing the  
452 largest scales of turbulence. This last remark leads to two conclusions. First, it is confirmed that in the FT region, no  
453 oscillatory motion is present or detectable by POD since the removal of low order modes immediately translates into a  
454 removal of large turbulent structures. Second, the importance of defining relevant criterion for the identification of  
455 oscillatory motion in grid stirred tank is further stressed out.

456 The simple use of a threshold mode number below which motion would be oscillatory and above which fluctuations  
457 would be turbulent is not a satisfactory solution. It can indeed, in some cases where oscillatory motion is weak, lead to a  
458 misrepresentation of turbulence properties.

## 459 4 | CONCLUSIONS

460 In water and DPS, most of the kinetic energy of the flow is contained in the first POD modes. This is especially true  
461 for regions of the flow close to or containing the grid's swept zone since in this region, the flow is governed by large  
462 coherent structures created by the grid's motion which are described by the first modes of the decomposition. The  
463 energetic dominance of the first modes is enhanced by the presence of polymer. The enhanced dominance of the first  
464 modes in DPS is a feature that can not be only attributed to the forcing of the flow, but that is also significant in purely  
465 turbulent regions. It endorses the idea that the small structures of turbulence (here represented by the high mode  
466 numbers) are significantly damped in dilute polymer solutions as observed previously<sup>43</sup>. Whether this effect is here due  
467 to viscosity or to non-Newtonian properties is still open for discussion. The effect of polymer seems to be felt differently

468 depending on the region: close to the grid it acts on the shape of organized motion, far from the grid on the structure of  
469 turbulence.

470 Criterion for the identification of organized motion in stirred tanks based on eigenvalue spectrum and temporal  
471 coefficient mostly fail to reveal oscillatory motion in OGT. This is not surprising in the FT region, since it is assumed  
472 that the intensity of oscillatory motion quickly decreases when moving away from the grid. Without identifying  
473 precisely the modes associated to oscillatory motion, defining an arbitrary cut-off mode number is obviously not fully  
474 satisfactory: removing the first POD modes leads to artificially remove kinetic energy from the reconstructed flow, and  
475 to a modification of the power spectra. Modes in the GN region shows only weak if any sign of oscillatory behaviour.  
476 This is consistent with the fact that the periodic motion evidenced in phase resolved measurements was quite weak  
477 energetically compared to periodic motion in the SZ region<sup>40</sup>.

478 In this SZ region however, oscillatory motion is known to be strong. Even if two-mode coupling is not as clear as in  
479 stirred tanks, a different type of coupling involving at least three modes seems to appear. The exact reasons to why the  
480 link between mode coupling and oscillatory motion seems more complex in the OGT situations than in stirred tank are  
481 yet to be understood. A first guess can be advanced: in POD studies applied to stirred tanks, the motion of the blade is  
482 always in the same direction. The oscillatory motion, that is to say vortex shedding by the blade, is thus always the same  
483 (same vortex propagation direction and rotation), and appears periodically. In the OGT case however, oscillatory eddies  
484 rotation is reversed whether the grid goes up or down. In the stirred tank case, turbulent structures once generated by  
485 the blade evolve and dissipate freely in its wake. In the grid-stirred case on the other hand, eddies generated by one  
486 grid pass almost immediately re-interact with the grid half a period later. All the above strongly could make the model  
487 description more complex, likely to be associated with a (chaotic) near-grid mixing process efficient at low Reynolds  
488 numbers.

489 A visual summary of the previous conclusions is made in figure 10.

490 It is well known that POD is useful to identify coherent fluid structures in various type of flows. In this work, we  
491 showed that the criterion for periodic flow identification may not always succeed. However POD still allows to isolate  
492 and remove flow features that are not purely intrinsic to turbulence from subsequent analysis, and avoid the pitfall  
493 of misinterpreting coherent fluctuations for turbulence. This is a first and crucial step towards proper modelling of  
494 turbulence properties in such flows.

495 Further investigations on the POD study of OGT should focus on this issue of oscillatory motion identification using  
496 modes. The structures observed on 3 modes temporal coefficient scatter plots suggest that a more complex mode  
497 coupling may exist, and so that criterion could be developed to identify periodic flows from POD decomposition in grid  
498 stirred tanks. This development of more universal criterion is of great interest for in the investigations of non-Newtonian  
499 effects on flow organization and oscillatory motion in grid stirred tanks, but also in more complex situations involving  
500 periodic forcing. Polymer concentration effect could then be investigated quite easily, even if a first simple approach  
501 using the tools of eigenvalue spectrum and Newtonian-normalized eigenvalue spectrum can also be considered (figure  
502 3). The use of a dynamic modes decomposition method (DMD,<sup>49,2018de Lamotte et al.de Lamotte, Delafosse, Calvo, and Tøye</sup>) could  
503 also be considered as an interesting alternative to access additional information on temporal variation, despite the low  
504 temporal resolution of the data.

505 Finally, the similarities between the pattern observed in figure 7 for the SZ region and the shape of chaotic attractors  
506 and associated trajectories raises an interesting question: the possible existence of an underlying chaotic process in  
507 oscillating grid flows, that may be present in laminar cases and persist in turbulent cases, in the grid swept zone. Further  
508 works could be done in this sense.

## ACKNOWLEDGEMENTS

The authors thank Dr. Gaby Launay, Dr. Neil Cagney and the two anonymous reviewers for their constructive remarks and feedback.

## REFERENCES

- [1] R. P. Chhabra and John Francis Richardson. Non-Newtonian Flow in the Process Industries: Fundamentals and Engineering Applications. Butterworth-Heinemann, 1999.
- [2] Joseph Kukura, Paulo Campos Arratia, Edit S. Szalai, Kevin J. Bittorf, and Fernando J. Muzzio. Understanding pharmaceutical flows. Pharmaceutical technology, 26(10):48–73, 2002.
- [3] J.-C. Gabelle, F. Augier, A. Carvalho, R. Rousset, and J. Morchain. Effect of tank size on  $kLa$  and mixing time in aerated stirred reactors with non-newtonian fluids. The Canadian Journal of Chemical Engineering, 89(5):1139–1153, October 2011.
- [4] J.-C. Gabelle, J. Morchain, D. Anne-Archard, F. Augier, and A. Liné. Experimental determination of the shear rate in a stirred tank with a non-newtonian fluid: Carbopol. AIChE Journal, 59(6):2251–2266, June 2013.
- [5] Rajendra P. Chhabra. Non-Newtonian Fluids: An Introduction. In Rheology of Complex Fluids, pages 3–34. Springer, New York, NY, 2010.
- [6] A. Liberzon, M. Guala, W. Kinzelbach, and A. Tsinober. On turbulent kinetic energy production and dissipation in dilute polymer solutions. Physics of Fluids, 18(12):125101, December 2006.
- [7] E. De Angelis, C. M. Casciola, R. Benzi, and R. Piva. Homogeneous isotropic turbulence in dilute polymers. Journal of Fluid Mechanics, 531:1–10, May 2005.
- [8] Alex Liberzon. On the effects of dilute polymers on driven cavity turbulent flows. International Journal of Heat and Fluid Flow, 32(6):1129–1137, December 2011.
- [9] M. Quan Nguyen, Alexandre Delache, Serge Simoëns, Wouter J. T. Bos, and Mamoud EL Hajem. Small scale dynamics of isotropic viscoelastic turbulence. Physical Review Fluids, 1(8):083301, December 2016.
- [10] Katepalli R. Sreenivasan and Christopher M. White. The onset of drag reduction by dilute polymer additives, and the maximum drag reduction asymptote. Journal of Fluid Mechanics, 409:149–164, April 2000.
- [11] Victor Voulgaropoulos, Ivan Zadrazil, Niccolò Le Brun, Alexander Bismarck, and Christos N. Markides. On the link between experimentally-measured turbulence quantities and polymer-induced drag reduction in pipe flows. AIChE Journal, 65(9):e16662, 2019.
- [12] P. E. Arratia, J. Kukura, J. Lacombe, and F. J. Muzzio. Mixing of shear-thinning fluids with yield stress in stirred tanks. AIChE Journal, 52(7):2310–2322, July 2006.
- [13] Fanny Rasschaert, Emeline Talansier, Didier Blésès, Albert Magnin, and Maud Lambert. Packaging of yield stress fluids: Flow patterns. AIChE Journal, 64(3):1117–1126, 2018.
- [14] A. Liné, J. C. Gabelle, J. Morchain, D. Anne-Archard, and F. Augier. On POD analysis of PIV measurements applied to mixing in a stirred vessel with a shear thinning fluid. Chemical Engineering Research and Design, 91(11):2073–2083, November 2013.
- [15] Evan A. Variano and Edwin A. Cowen. Turbulent transport of a high-Schmidt-number scalar near an air–water interface. Journal of Fluid Mechanics, 731:259–287, September 2013.

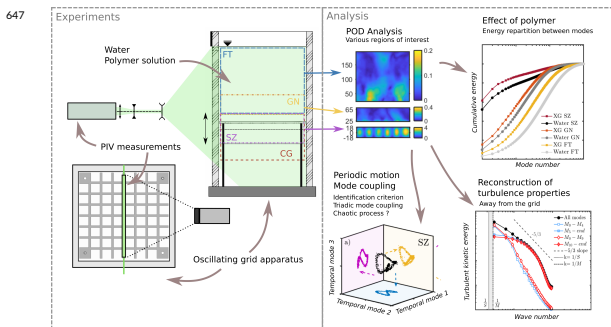


- 546 [16] G. Cocconi, E. De Angelis, B. Frohnapfel, M. Baevsky, and A. Liberzon. Small scale dynamics of a shearless turbulent/non-  
547 turbulent interface in dilute polymer solutions. Physics of Fluids, 29(7):075102, July 2017.
- 548 [17] Alice M. Crawford, Nicolas Mordant, Haitao Xu, and Eberhard Bodenschatz. Fluid acceleration in the bulk of turbulent  
549 dilute polymer solutions. New Journal of Physics, 10(12):123015, 2008.
- 550 [18] S. M. Thompson and J. S. Turner. Mixing across an interface due to turbulence generated by an oscillating grid. Journal  
551 of Fluid Mechanics, 67(02):349–368, January 1975.
- 552 [19] E. J. Hopfinger and J.-A. Toly. Spatially decaying turbulence and its relation to mixing across density interfaces. Journal  
553 of Fluid Mechanics, 78(01):155–175, November 1976.
- 554 [20] S. I. Voropayev and H. J. S. Fernando. Propagation of grid turbulence in homogeneous fluids. Physics of Fluids, 8(9):  
555 2435–2440, September 1996.
- 556 [21] H. Herlina. Gas transfer at the air-water interface in a turbulent flow environment. PhD thesis, Universitätsverlag Karl-  
557 ruhe, Karlsruhe, June 2005.
- 558 [22] Mark W. McCorquodale and R. J. Munro. Experimental study of oscillating-grid turbulence interacting with a solid bound-  
559 ary. Journal of Fluid Mechanics, 813:768–798, February 2017.
- 560 [23] Mark W. McCorquodale and R. J. Munro. Analysis of intercomponent energy transfer in the interaction of oscillating-grid  
561 turbulence with an impermeable boundary. Physics of Fluids, 30(1):015105, January 2018.
- 562 [24] Blair H. Brumley and Gerhard H. Jirka. Near-surface turbulence in a grid-stirred tank. Journal of Fluid Mechanics, 183:  
563 235–263, October 1987.
- 564 [25] S. P. McKenna and W. R. McGillis. The role of free-surface turbulence and surfactants in air–water gas transfer. International Journal of Heat and Mass Transfer, 47(3):539–553, January 2004.
- 565 [26] Luca Chiapponi, Sandro Longo, and Mara Tonelli. Experimental study on oscillating grid turbulence and free surface  
566 fluctuation. Experiments in Fluids, 53(5):1515–1531, September 2012.
- 567 [27] Tom Lacassagne, Mahmoud EL Hajem, Fabien Morge, Serge Simoens, and Jean-Yves Champagne. Study of Gas Liquid  
568 Mass Transfer in a Grid Stirred Tank. Oil & Gas Science and Technology – Revue d'IFP Energies nouvelles, 72(1):7, January  
569 2017. doi: 10.2516/ogst/2017001.
- 570 [28] E Xuequan and E. J. Hopfinger. On mixing across an interface in stably stratified fluid. Journal of Fluid Mechanics, 166:  
571 227–244, May 1986.
- 572 [29] Lilly Verso, Maarten van Reeuwijk, and Alex Liberzon. Steady state model and experiment for an oscillating grid turbulent  
573 two-layer stratified flow. Physical Review Fluids, 2(10):104605, October 2017.
- 574 [30] Yasuyuki Nagami and Takayuki Saito. An Experimental Study of the Modulation of the Bubble Motion by Gas–Liquid-  
575 Phase Interaction in Oscillating-Grid Decaying Turbulence. Flow, Turbulence and Combustion, 92(1-2):147–174,  
576 September 2013.
- 577 [31] Lei San, Tianyu Long, and Clark C. K. Liu. Algal Bioproductivity in Turbulent Water: An Experimental Study. Water, 9(5):  
578 304, April 2017.
- 579 [32] Marie Rastello, Hervé Michallet, and Jean-Louis Marié. Sediment erosion in zero-mean-shear turbulence. Coastal  
580 Dynamics, (094):597–607, 2017.
- 581 [33] Alan J. S. Cuthbertson, Farzin Samsami, and Ping Dong. Model studies for flocculation of sand-clay mixtures. Coastal  
582 Engineering, 132:13–32, February 2018.
- 583

- 584 [34] M. T. Mahamod, W. H. M. Wan Mohtar, and S. F. M. Yusoff. Spatial and temporal behavior of pb, cd and zn release during  
585 short term low intensity resuspension events. Jurnal Teknologi, 80(1), December 2017.
- 586 [35] Trevor J. Mcdougall. Measurements of turbulence in a zero-mean-shear mixed layer. Journal of Fluid Mechanics, 94(03):  
587 409–431, October 1979.
- 588 [36] R. I. Nokes. On the entrainment rate across a density interface. Journal of Fluid Mechanics, 188:185–204, March 1988.
- 589 [37] I. P. D. De Silva and H. J. S. Fernando. Some aspects of mixing in a stratified turbulent patch. Journal of Fluid Mechanics,  
590 240:601–625, July 1992.
- 591 [38] Chia Ren Chu and Gerhard H. Jirka. Turbulent gas flux measurements below the air-water interface of a grid-stirred tank.  
592 International Journal of Heat and Mass Transfer, 35(8):1957–1968, August 1992.
- 593 [39] N. Matsunaga, Y. Sugihara, T. Komatsu, and A. Masuda. Quantitative properties of oscillating-grid turbulence in a homo-  
594 geneous fluid. Fluid Dynamics Research, 25(3):147–165, September 1999.
- 595 [40] Tom Lacassagne, Adrien Lyon, Serge Simoëns, Mahmoud El Hajem, and Jean-Yves Champagne. Flow around an oscillating  
596 grid in water and shear-thinning polymer solution at low Reynolds number. Experiments in Fluids, 61(1):15, December  
597 2019.
- 598 [41] A. Liberzon, M. Holzner, B. Lüthi, M. Guala, and W. Kinzelbach. On turbulent entrainment and dissipation in dilute poly-  
599 mer solutions. Physics of Fluids (1994-present), 21(3):035107, March 2009.
- 600 [42] Yue Wang, Wei-Hua Cai, Tong-Zhou Wei, Lu Wang, and Feng-Chen Li. Experimental Study on Two-Oscillating Grid Tur-  
601 bulence With Polymer Additives. page V001T15A008, Seoul, South Korea, July 2015. ASME.
- 602 [43] Yue Wang, Wei-Hua Cai, Tong-Zhou Wei, Hong-Na Zhang, Lu Wang, and Feng-Chen Li. Proper orthogonal decompo-  
603 sition analysis for two-oscillating grid turbulence with viscoelastic fluids. Advances in Mechanical Engineering, 8(11):  
604 1687814016679773, November 2016.
- 605 [44] W. D. McComb, J. Allan, and C. A. Greated. Effect of polymer additives on the small-scale structure of grid-generated  
606 turbulence. The Physics of Fluids, 20(6):873–879, June 1977.
- 607 [45] Richard Vonlanthen and Peter A. Monkewitz. Grid turbulence in dilute polymer solutions: PEO in water. Journal of Fluid  
608 Mechanics, 730:76–98, September 2013.
- 609 [46] Tom Lacassagne, Serge Simoëns, Mahmoud EL Hajem, Adrien Lyon, and Jean-Yves Champagne. Oscillating grid turbu-  
610 lence in shear-thinning polymer solutions. Physics of Fluids, 31(8):083102, August 2019.
- 611 [47] Renaud Escudié and Alain Liné. Experimental analysis of hydrodynamics in a radially agitated tank. AIChE Journal, 49  
612 (3):585–603, March 2003.
- 613 [48] Andrea Ducci, Zacharias Doulgerakis, and Michael Yianneskis. Decomposition of Flow Structures in Stirred Reactors and  
614 Implications for Mixing Enhancement. Industrial & Engineering Chemistry Research, 47(10):3664–3676, May 2008.
- 615 [49] Anne de Lamotte, Angélique Delafosse, Sébastien Calvo, and Dominique Toye. Analysis of PIV measurements using  
616 modal decomposition techniques, POD and DMD, to study flow structures and their dynamics within a stirred-tank re-  
617 actor. Chemical Engineering Science, 178:348–366, March 2018.
- 618 [50] Laurent Graftieux, Marc Michard, and Nathalie Grosjean. Combining PIV, POD and vortex identification algorithms for  
619 the study of unsteady turbulent swirling flows. Measurement Science and Technology, 12(9):1422, 2001.
- 620 [51] Jean-Christophe Gabelle, Jérôme Morchain, and Alain Liné. Kinetic Energy Transfer between First Proper Orthogonal  
621 Decomposition Modes in a Mixing Tank. Chemical Engineering & Technology, 40(5):927–937, May 2017.

- 622 [52] Jana Hamdi, Hassan Assoum, Kamel Abed-Meraim, and Anas Sakout. Volume reconstruction of an impinging jet obtained  
623 from stereoscopic-PIV data using POD. European Journal of Mechanics - B/Fluids, 67:433–445, January 2018.
- 624 [53] Tom Lacassagne. Oscillating grid turbulence and its influence on gas liquid mass transfer and mixing in non-Newtonian  
625 media. PhD Thesis, University of Lyon, INSA Lyon, 2018.
- 626 [54] Johannes G. Janzen, H. Herlina, Gerhard H. Jirka, Harry E. Schulz, and John S. Gulliver. Estimation of mass transfer  
627 velocity based on measured turbulence parameters. AIChE Journal, 56(8):2005–2017, August 2010.
- 628 [55] Nicholas B. Wyatt and Matthew W. Liberatore. Rheology and viscosity scaling of the polyelectrolyte xanthan gum.  
629 Journal of Applied Polymer Science, 114(6):4076–4084, December 2009.
- 630 [56] A. K. M. F. Hussain and W. C. Reynolds. The mechanics of an organized wave in turbulent shear flow. Journal of Fluid  
631 Mechanics, 41(2):241–258, April 1970.
- 632 [57] Lawrence Sirovich. Turbulence and the dynamics of coherent structures. I. Coherent structures. Quarterly of applied  
633 mathematics, 45(3):561–571, 1987.
- 634 [58] J. Moreau and A. Liné. Proper orthogonal decomposition for the study of hydrodynamics in a mixing tank. AIChE Journal,  
635 52(7):2651–2655, July 2006.
- 636 [59] X. Xie, N. Dietrich, L. Fillaudeau, C. Le Men, P. Schmitz, and A. Liné. Local Hydrodynamics Investigation within a Dynamic  
637 Filtration Unit under Laminar Flow. Chemical Engineering Research and Design, February 2018.
- 638 [60] LaVision. DaVIs Flowmaster Manual. LaVision GmbH, 2011.
- 639 [61] Elisabetta De Angelis, Carlo M. Casciola, Victor S. L'vov, Renzo Piva, and Itamar Procaccia. Drag reduction by polymers  
640 in turbulent channel flows: Energy redistribution between invariant empirical modes. Physical Review E, 67(5):056312,  
641 May 2003.
- 642 [62] A. Liné. Eigenvalue spectrum versus energy density spectrum in a mixing tank. Chemical Engineering Research and  
643 Design, 108:13–22, April 2016.
- 644 [63] J M Ottino. Mixing, Chaotic Advection, and Turbulence. Annual Review of Fluid Mechanics, 22(1):207–254, 1990.
- 645 [64] S. B. Pope. Turbulent Flows. Cambridge University Press, August 2000.

## 646 GRAPHICAL ABSTRACT



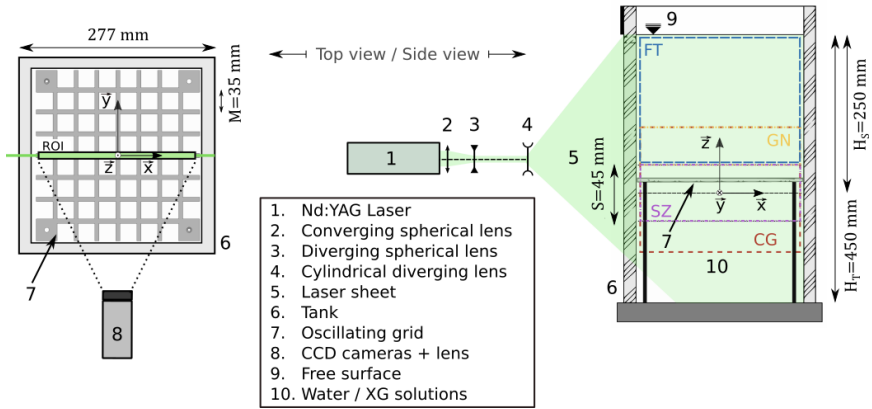


**FIGURE 1** Sketch of the experimental setup and of the regions of study: SZ for Swept Zone, GN for Grid Neighborhood, CG for Close Grid, FT for full tank.

Study	Close grid	Full tank
$\Delta t$ (ms)	4	18
$f_{acq}$ (Hz)	10	4
Interrogation window size (px-px)	48-48, 24-24	64-64, 32-32
Camera-plane distance (mm)	300-400	800-1000
f-number	16	16
Spatial resolution (mm)	3.4	2.3

**TABLE 1** Parameters for PIV study of oscillating grid turbulence. Spatial resolution denotes the distance between two PIV computed vectors (same along X and Z).

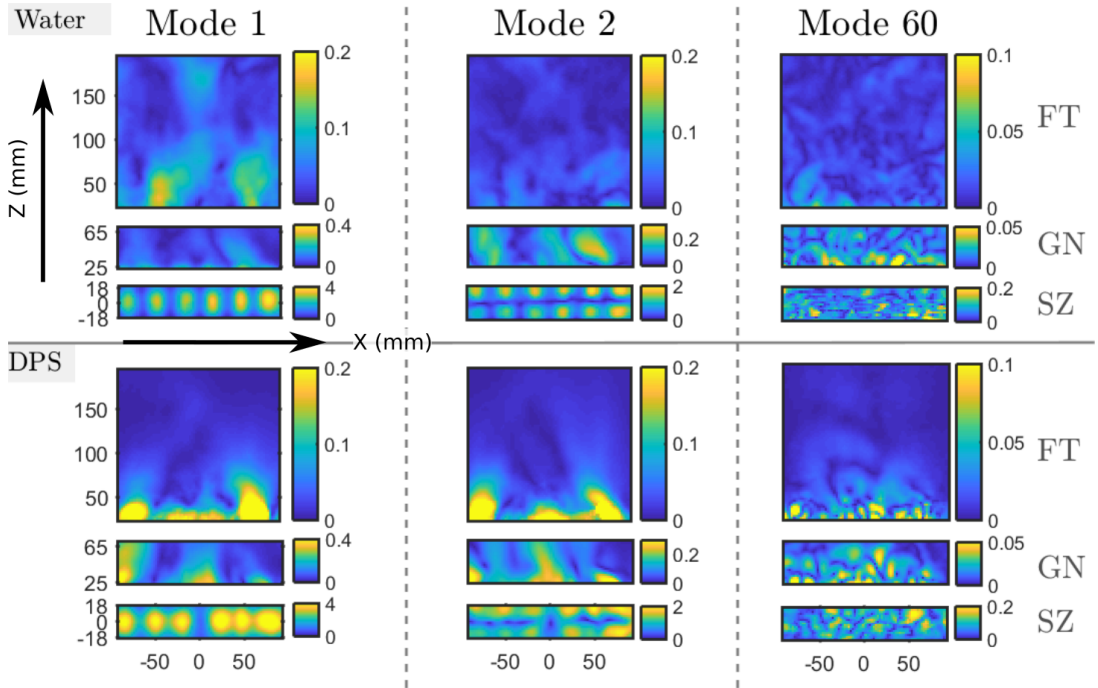


**FIGURE 2** Example of spatial POD modes: modes 1,2 and 60 for regions "Swept Zone" (SZ), "Grid Neighbourhood" (GN) and "Full Tank" (FT), in water (top half) and DPS at 100 ppm concentration (bottom half). The colormap represents the local non dimensional mode magnitude  $\sqrt{(\phi_x^i)^2 + (\phi_z^i)^2}$ . Note that these are not reconstructed velocity magnitudes. The velocity intensity is carried by the temporal mode coefficients and modulated by the present maps. The above color maps should not be used to compare one mode amplitude to another, but only between spatial structures of the modes.

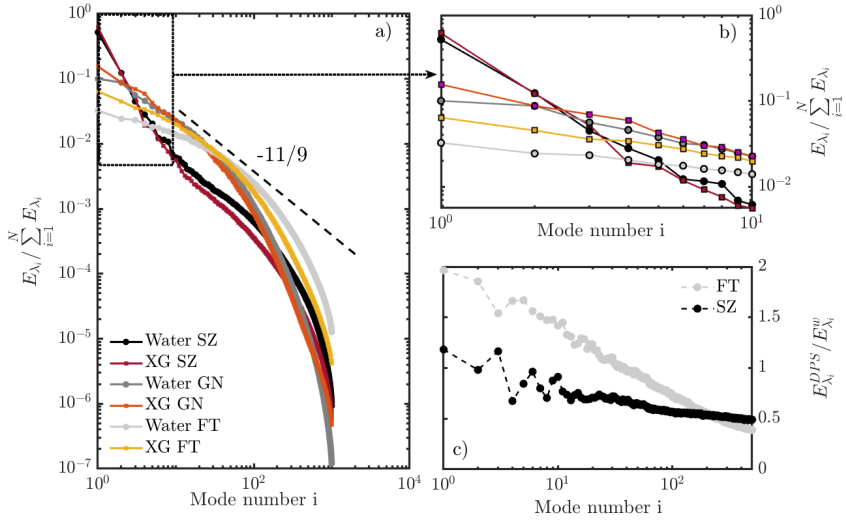


**FIGURE 3** POD eigenvalue spectrum. a) Full spectrum, b) zoom on the first 10 modes. c) POD eigenvalue spectrum of dilute polymer solution normalized by the water spectrum for FT and SZ regions.

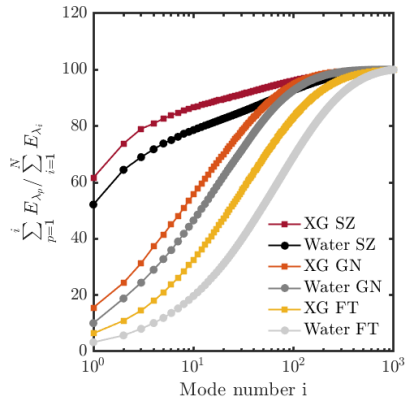


**FIGURE 4** Cumulative energy contained in the POD modes,  $i$  axis in log scale

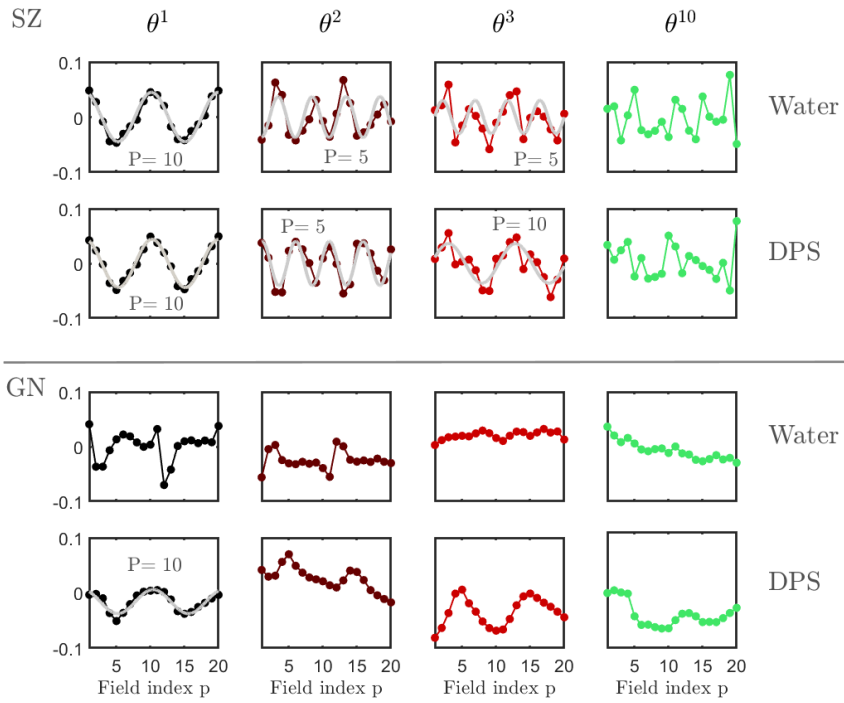


**FIGURE 5**  $\theta^i$  coefficients as a function of the instantaneous field index. Modes 1, 2 and 3 are represented as modes for which a periodic behavior can be expected. Mode 10 (chosen arbitrarily among highest mode numbers) is used as a reference for non periodic modes. Superimposed light gray lines are best sinusoidal fittings using the full series of snapshots for modes exhibiting a periodic behaviour. The period  $P$  of each sinusoidal fitting, expressed in field numbers, is indicated in each plots.

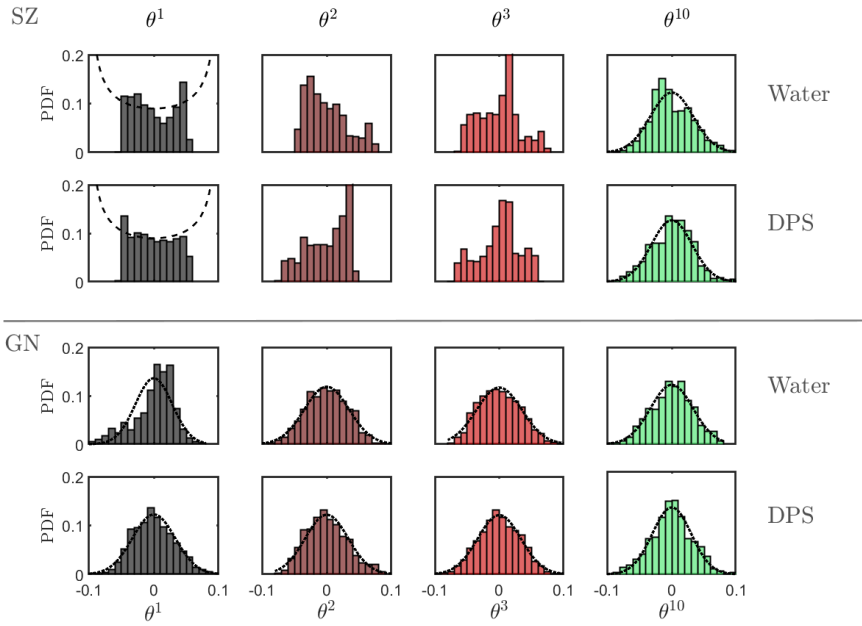


**FIGURE 6** Histogram plot of  $\theta^i$  coefficient values (arbitrary units) for 1000 instantaneous velocity fields. The same modes as figure 5 are represented. Dotted lines and dashed lines are fittings of PDFs by respectively Gaussian functions (for apparently random modes) and Sinusoidal PDF trend (for apparently periodic modes). No trend lines are shown for modes with hybrid behavior ( $\theta^2$  and  $\theta^3$  in SZ).

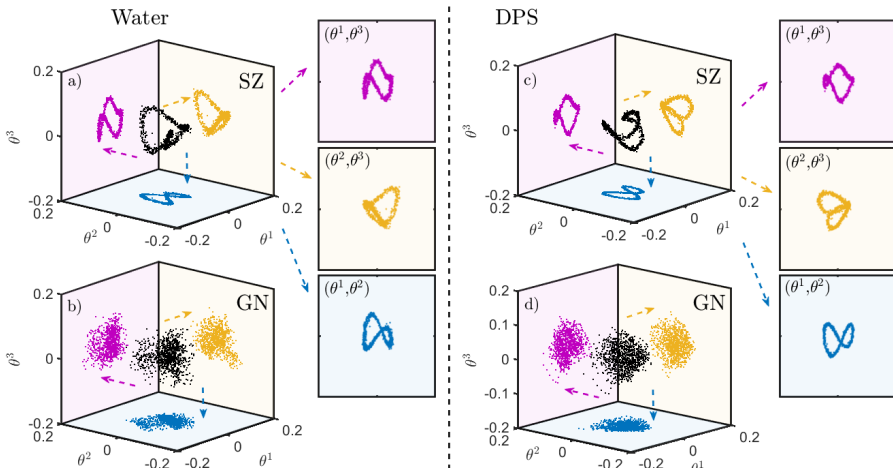


**FIGURE 7** Scatter plots of  $(\theta_1, \theta_2, \theta_3)$  for water (a,b) and DPS (c,d) in the SZ (a,c) and GN (b,d) regions. 2D projections in planes  $(\theta_1, \theta_2)$  (blue),  $(\theta_2, \theta_3)$  (yellow), and  $(\theta_1, \theta_3)$  (purple) are shown in figures a to d and extracted for sub-figures a) and c).



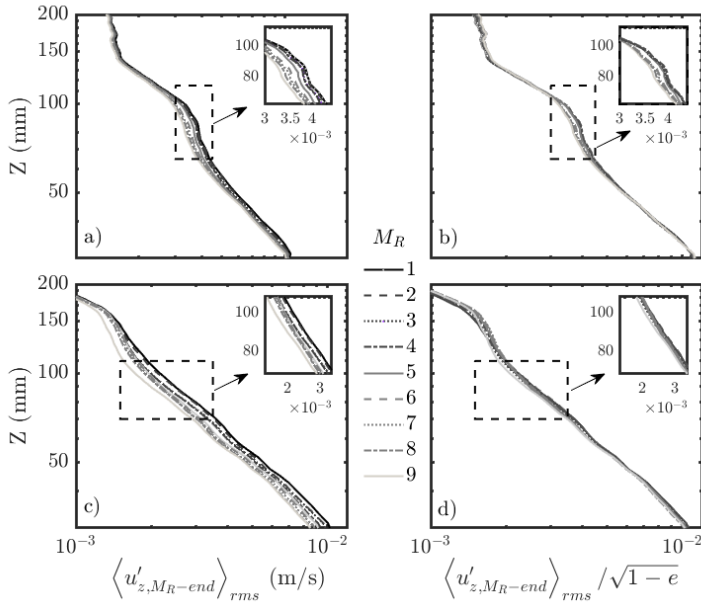


**FIGURE 8** Reconstructed rms profiles  $\langle u'_{z, M_R - end} \rangle_{rms}$  for water (a,b) and DPS (c,d) after removal of the first  $M_R$  modes,  $M_R = 1$  to  $M_R = 9$ . a) and c) are reconstructed rms profiles, and b) and d) reconstructed profiles scaled to account for energy removal. Inserted sub-figures correspond to zooms on regions evidenced by dashed rectangle.

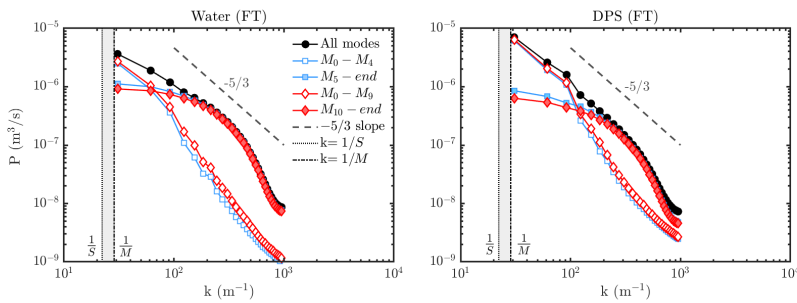


**FIGURE 9** POD reconstruction of turbulence total power spectrum  $P = P_l + P_t$  using all the modes (black dots), modes 0 to 4 (empty blue squares), modes 5 and above (full blue squares), modes 0 to 9 (empty red diamonds), and modes 10 and above (full red diamonds). The grid energy input occurs at wave numbers between  $1/S$  and  $1/M$  (gray region). The expected inertial sub-range power law slope is also represented (dashed line).

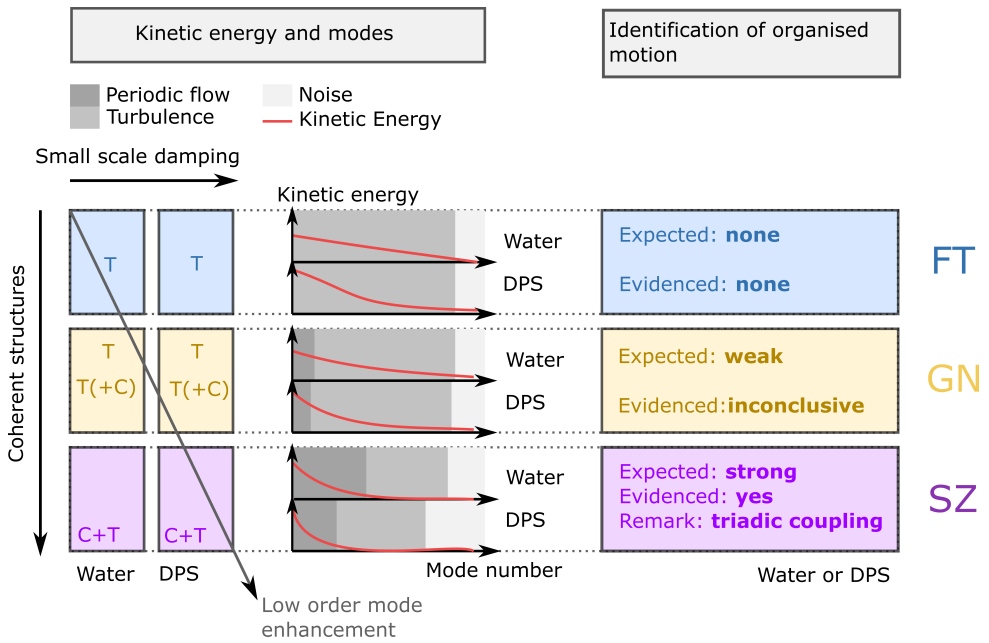


**FIGURE 10** Visual summary of the main conclusions of the present study regarding kinetic energy distribution in modes as a function of region of interest or fluid considered (left columns), and identification of organised motion (right column).